Research of Extra Charged Gauge Boson *W′* in Alternative Left-Right Model at Future Muon Collider*

Liuxin Zhao (赵刘欣)   Honglei Li (李洪蕾)[†]   Zhi-Long Han (韩志龙)[‡]   Fei Huang (黄飞)[§]   Xinyi Yan (闫心怡)

School of Physics and Technology, University of Jinan, 250022, Jinan, China

Abstract: The study of extra charged gauge boson beyond the Standard Model has always been of great interest. Future muon colliders will have a significant advantage in discovering exotic particles. In this paper, by studying the $\mu^+\mu^- \to W'^+W'^- \to e^+e^-n_e\bar{n}_e$ process, we explore the properties of *W′* in the alternative left-right model. The cross section and angular distribution of the final electron are investigated in the scenario of different *W′* mass and right-handed coupling constant. The forward-backward asymmetry is also an important observable to reflect the properties of *W′*. We provide a method to effectively suppress the background processes by imposing constraints on the transverse momentum P_T and azimuthal angle of the final-state electrons α. With the cuts of $600 < P_T < 3500$ GeV and $0.5 < \alpha < 3$, the significance can beyond 5σ for 4.8 TeV *W′* at the collision energy of 10 TeV.

Keywords: new gauge boson, muon collider, Alternative Left-Right Model

DOI: **CSTR:** 32044.14.ChinesePhysicsC.

I. INTRODUCTION

The exploration of new physics is an active field in particle physics, aiming to go beyond the limitations of the Standard Model (SM) and solve mysteries such as dark matter, dark energy, and the mass of neutrino, etc. Among them, supersymmetry theory (SUSY) [1−3] grand unified theory (GUT) [4−6], extra dimension theory and related extended theories [7−11] are the popular theories in the process of new physics research. Additional gauge particles are predicted along with the new gauge group involved. The detection of the *W′* particle is an important goal in new physics models. Recently, the CDF experiment group at Fermilab, through precise measurements of the *W* boson mass, found deviations from the expectations of the Standard Model [12]. The *W* mass anomaly can be explained in 3-3-1 model, and in 3-3-1 model there exist *W′* particle [13].

The *W′* particle was proposed mainly to address some of the limitations and mysteries of the Standard Model. It is a hypothetical particle beyond the predictions of the Standard Model, resulting from new theories and models, and the properties of the *W′* particle have different predictions in different models. The origin and background of the *W′* particle are closely related to the electroweak symmetry breaking and the Higgs mechanism. In the Standard Model, *W* and *Z* bosons acquire masses through the Higgs mechanism. If the *W′* particle exists, it may involve a relatively more complex mode of symmetry breaking. Therefore, the existence of the *W′* particle may point to new phenomena, such as the aforementioned GUT, extra dimension theory, which provide a possible framework to explain the properties of the *W′* particle and its interactions with other particles. The alternative left-right model is an attractive model from GUT symmetry breaking, which provides the explanation of neutrino masses and dark matter candidates. We choose the alternative left-right model for the studies of *W′*. In this model, the *W′* particle can allow for the existence of light masses, and its mass is influenced by the coupling constants. The ratio of $M_{W'}/M_{Z'}$ depends on the right-handed coupling constant g_R. The model introduces a *S* symmetry, which provides theoretical stability for the newly neutral fermions and Higgs particles that can serve as dark matter candidates [14, 15]. At the same time, the model avoids flavor-changing neutral currents, which allows for the charged bosons to be light. One can study the interactions of *W′* with the Standard Model particles and

further explore the dark matter interactions with the W' particle as a mediator, and so on. Overall, the exploration of the W' particle is an exciting field in particle physics. It may not only reveal clues to new physics [16−23] but also provide us with the key to a deeper understanding of the universe. In the coming years, we are looking forward to further exploration of the W' particle in the future colliders.

In this paper, we firstly introduce the relevant research content related to W' particles. In the second section, we focus on the model building of this study and the current mass constraints of W' particle. In the third section, we investigate the process $\mu^+\mu^- \to W'^+ W'^- \to e^+ e^- n_e \bar{n}_e$ at the future muon collider. Finally, a brief summary is given.

II. W' IN THE ALTERNATIVE LEFT-RIGHT MODEL AND THE CONSTRAINTS

The research of grand unified theory (GUT) is widely popular, originating from the symmetry breaking of the E_6 group [24, 25]. The group of $SO(10) \times U(1)$ and $SU(3) \times SU(3) \times SU(3)$ are two of the many subgroups of the E_6 group, where the classical left-right symmetric model arises from the $SO(10) \times U(1)$ group structure [26, 27]. And the alternative left-right model (ALRM) [10, 28] discussed in the work is obtained by the breaking chain of the $SU(3) \times SU(3) \times SU(3)$ subgroup.

The quantum numbers and representations selected for the fermionic field content of the ALRM are inspired by heterotic superstring models [10]. With the largest subgroup $SU(3)_C \times SU(3)_L \times SU(3)_H$ of E_6, there has 27 representation to display the particles

$$27 = (3,3,1) + (\bar{3},1,\bar{3}) + (1,\bar{3},3) \equiv q + \bar{q} + l. \quad (1)$$

The alternative left-right model is based on the $SU(3)_C \times SU(2)_L \times SU(2)_{R'} \times U(1)_{B-L} \times S$ gauge group. In this context, the $SU(3)_C$ group represents the symmetry group of the strong interaction, corresponding to the strong force that binds quarks together. $SU(2)_L$ is the symmetry of the weak interaction for left-handed particles. $SU(2)_{R'}$ is the symmetry of the weak interaction for right-handed particles and S is a discrete symmetry imposed to distinguish between scalar and dual scalar fields. Initially, the gauge and global symmetry group $SU(2)_{R'} \times U(1)_{B-L} \times S$ of ALRM is broken to produce the hypercharge $U(1)_Y$. The symmetry breaking is achieved through the $SU(2)_{R'}$ doublet of scalar fields χ_R, which are charged under S. To maintain left-right symmetry, an $SU(2)_L$ doublet of scalar fields χ_L is introduced. However, unlike χ_R, χ_L does not couple with S. The electroweak symmetry is further broken down to electromagnetism through a bidoublet Higgs field that

carries charges under both $SU(2)_L$ and $SU(2)_{R'}$, but has no $B-L$ quantum numbers. This Higgs field is non-trivial under both $SU(2)_L$ and $SU(2)_{R'}$ transformations but does not affect the $B-L$ symmetry [11]. We represent it with a more intuitive process as follows

$$SU(2)_L \times SU(2)_{R'} \times U(1)_{B-L} \times S \xrightarrow{\langle \chi_R \rangle} SU(2)_L$$
$$\times U(1)_Y \xrightarrow{\langle \Phi \rangle, \langle \chi_L \rangle} U(1)_{EM}. \quad (2)$$

The particles of ALRM with the representation of field are listed in Table 1.

Under the S symmetry, there are some odd S symmetry particles: the scotinos n_L, n_R, the exotic quarks d'_L, d'_R, the gauge boson W', and the scalar particles. The Yukawa Lagrangian of ALRM is written as

$$\mathcal{L}_Y = \bar{Q}_L Y^q \tilde{\Phi} Q_R + \bar{Q}_L Y^q_L \chi_L d_R + \bar{Q}_R Y^q_R \chi_R d'_L$$
$$+ \bar{L}_L Y^\ell \Phi L_R + \bar{L}_L Y^\ell_L \tilde{\chi}_L \nu_R + \bar{L}_R Y^\ell_R \tilde{\chi}_R n_L + h.c., \quad (3)$$

where Y is a 3×3 matrix of Yukawa couplings, with subscripts L and R representing the left-handed and right-handed coupling matrices respectively, and superscripts q and l representing the quarks and leptons in the model. The vacuum expectation values (vevs) of the scalar fields is expressed as

Table 1. Field content of the ALRM and respective quantum numbers.

Fields	$SU(3)_C \times SU(2)_L \times SU(2)_{R'} \times U(1)_{B-L}$	S
Fermions		
$Q_L = \begin{pmatrix} u \\ d \end{pmatrix}_L$	$\left(3, 2, 1, +\frac{1}{6}\right)$	0
$Q_R = \begin{pmatrix} u \\ d' \end{pmatrix}_R$	$\left(3, 1, 2, +\frac{1}{6}\right)$	$-\frac{1}{2}$
d'_L	$\left(3, 1, 1, -\frac{1}{3}\right)$	-1
d_R	$\left(3, 1, 1, -\frac{1}{3}\right)$	0
$L_L = \begin{pmatrix} \nu \\ e \end{pmatrix}_L$	$\left(1, 2, 1, -\frac{1}{2}\right)$	0
$L_R = \begin{pmatrix} n \\ e \end{pmatrix}_R$	$\left(1, 1, 2, -\frac{1}{2}\right)$	$+\frac{1}{2}$
n_L	$\left(1, 1, 1, 0\right)$	$+1$
ν_R	$\left(1, 1, 1, 0\right)$	0
Higgs		
$\Phi = \begin{pmatrix} \phi^0_1 \phi^+_1 \\ \phi^-_2 \phi^0_2 \end{pmatrix}_R$	$\left(1, 2, 2^*, 0\right)$	$-\frac{1}{2}$
$X_L = \begin{pmatrix} \chi^+_L \\ \chi^0_L \end{pmatrix}_L$	$\left(1, 2, 1, +\frac{1}{2}\right)$	0
$X_R = \begin{pmatrix} \chi^+_R \\ \chi^0_R \end{pmatrix}_L$	$\left(1, 1, 2, +\frac{1}{2}\right)$	$+\frac{1}{2}$

$$\langle\Phi\rangle = \frac{1}{\sqrt{2}}\begin{pmatrix} 0 & 0 \\ 0 & k \end{pmatrix}, \quad \langle\chi_L\rangle = \frac{1}{\sqrt{2}}\begin{pmatrix} 0 \\ v_L \end{pmatrix},$$

$$\langle\chi_R\rangle = \frac{1}{\sqrt{2}}\begin{pmatrix} 0 \\ v_R \end{pmatrix}. \tag{4}$$

The masses of the gauge bosons are generated through the left-right symmetry breaking the Higgs mechanism. The masses of the charged bosons are the follows

$$M_W = \frac{1}{2}g_L\sqrt{k^2+v_L^2} \equiv \frac{1}{2}g_L v, \quad \text{and}$$

$$M_{W'} = \frac{1}{2}g_R\sqrt{k^2+v_R^2} \equiv \frac{1}{2}g_R v'. \tag{5}$$

However, due to $\langle\phi_1^0\rangle = 0$, the produced charged bosons will not mix, which means that the $W'^{\pm}$ and $W^{\pm}$ particles will maintain their respective characteristics and will not convert into each other.

The mass squared matrix of the neutral gauge bosons in the $\{W_{L\mu}^3, W_{R\mu}^3, B_\mu\}$ basis is

$$(\mathcal{M}_V^0)^2 = \frac{1}{4}\begin{pmatrix} g_{B-L}^2(v_L^2+v_R^2) & -g_{B-L}g_L v_L^2 & -g_{B-L}g_R v_R^2 \\ -g_{B-L}g_L v_L^2 & g_L^2 v^2 & -g_L g_R k^2 \\ -g_{B-L}g_R v_R^2 & -g_L g_R k^2 & g_R^2(v')^2 \end{pmatrix}, \tag{6}$$

where g_L, g_R and g_{B-L} are the gauge coupling constants of the $SU(2)_L, SU(2)_{R'}$ and $U(1)_{B-L}$ [29]. The matrix can be diagonalized through three rotations that mix the B, W_L^3, and W_R^3 bosons into the massless photon A and the massive Z and Z' states:

$$\begin{pmatrix} B_\mu \\ W_{L\mu}^3 \\ W_{R\mu}^3 \end{pmatrix} = \begin{pmatrix} \cos\phi_W & 0 & -\sin\phi_W \\ 0 & 1 & 0 \\ \sin\phi_W & 0 & \cos\phi_W \end{pmatrix} \begin{pmatrix} \cos\theta_W & -\sin\theta_W & 0 \\ \sin\theta_W & \cos\theta_W & 0 \\ 0 & 0 & 1 \end{pmatrix} \begin{pmatrix} 1 & 0 & 0 \\ 0 & \cos\zeta_W & -\sin\zeta_W \\ 0 & \sin\zeta_W & \cos\zeta_W \end{pmatrix} \begin{pmatrix} A_\mu \\ Z_\mu \\ Z'_\mu \end{pmatrix}, \tag{7}$$

where the ϕ_W rotation mixes the B and W_R^3 bosons into the hypercharge boson B, generated by the breaking of $SU(2)_{R'} \times U(1)_{B-L}$ into $U(1)_Y$. The θ_W represents the usual electroweak mixing, and the ζ_W rotation is related to the strongly constrained $Z-Z'$ mixing. The mass of the charged W' boson is indirectly constrained by the mass ratio $M_{W'}/M_{Z'} = c_{\phi W}$ [10], so the constraint of $M_{W'}$ is weaker than the LRSM.

In recent years, many research groups (such as the ATLAS Collaboration and the CMS Collaboration) have been actively exploring the experimental constraints on the mass of the W' particle, and have achieved a lot of research results [30−38]. Below are some of the latest research findings on the mass constraints of the W':

1. Bounds from CMS: The CMS Collaboration has searched for W' and heavy neutrino N_R with the signature of observing high transverse masses of the τ−lepton and missing transverse momentum at the LHC with $\sqrt{s} = 13$ TeV, corresponding to the integrated luminosity of 35.9 fb^{-1}. The mass bounds of W' is $M_{W'} \geq 4.0$ TeV, with the right-handed coupling equal to SM coupling [34]. But depending on the coupling in the non-universal $G(221)$ model, the bounds of heavy W' bosons is $M_{W'} \geq 1.7 \sim 3.9$ TeV [34]. Within the framework of the Sequential Standard Model, a W' boson with mass less than 5.3 TeV is excluded from the combined results of electron decay channels at the LHC with $\sqrt{s} = 13$ TeV [35]. The CMS collaboration utilizing data from Run 2 at the LHC has obtained constraints on the mass of the W' boson with Left-Right Symmetric Model at $\sqrt{s} = 13$ TeV. For the assumption of the right-handed neutrino masses equal to half the W' mass, the mass of W' is excluded at 95% confidence level up to 4.7 TeV and 5.0 TeV for the electron and muon channels [36].

2. Bounds from ATLAS: The ATLAS collaboration has searched for W' with observing at high transverse masses of the τ−lepton and missing transverse momentum at the LHC with $\sqrt{s} = 13$ TeV, corresponding to the integrated luminosity of 138 fb^{-1}. The present mass bounds of W' is $M_{W'} \geq 5.0$ TeV in Sequential Standard Model, with the right-handed coupling equal to SM coupling [37]. For the assumption of the coupling in the non-universal coupling $g_L \neq g_R$, the mass of W' is excluded at 95% confidence level up to $3.5 \sim 5.0$ TeV for the τ channel in the Sequential Standard Model. Corresponding to the integrated luminosity of 80 fb^{-1}, the mass of W' is excluded at 95% confidence level up to 4.8 TeV and 5.0 TeV for the electron and muon channels in the Left-Right Symmetric Model [38].

The constraints on the W' particle mentioned above come from the analysis of LHC data by various experimental groups using different models. Most current experimental results for W' particles primarily through the exploration of single production channels. Even when considering the pair production of W', the constraints on it become weaker. Therefore, we have chosen to investigate the properties of W' particles by exploring the signals of their pair production at the muon collider. This issue is closely related to our studied model. Most of the experimental results available today are based on sequential

Table 2. The mass constraints for W' from LHC.

|			
CMS	Sequential Standard Model [35]	$W' \to e^- \nu$	$M_{W'} \geq 5.3\,\mathrm{TeV}$
	Left-Right Symmetric Model [36]	$W' \to e^- N$	$M_{W'} \geq 4.7\,\mathrm{TeV}$
		$W' \to \mu^- N$	$M_{W'} \geq 5.0\,\mathrm{TeV}$
ATLAS	Sequential Standard Model($g_L = g_R$) [37]	$W' \to \tau^- \nu$	$M_{W'} \geq 5.0\,\mathrm{TeV}$
	Sequential Standard Model($g_L \neq g_R$) [37]	$W' \to \tau^- \nu$	$M_{W'} \geq 3.5 \sim 5.0\,\mathrm{TeV}$
	Left-Right Symmetric Model [38]	$W' \to e^- n_e$	$M_{W'} \geq 4.8\,\mathrm{TeV}$
		$W' \to \mu^- n_\mu$	$M_{W'} \geq 5.0\,\mathrm{TeV}$

models or the classical left-right symmetric model. In these models, the decay products of the newly introduced additional charged bosons are standard model particles (leptons or quarks). The mass of the W' boson is experimentally expected to be at least about 5.0 TeV, due to constraints from its dilepton decay channel at the LHC. However, in our study of the ALRM, the decay process of the W' boson couples to quark-exotic quark and charged lepton-scotino final states, which is a consequence of the discrete symmetry. In this model, we treat the scotino particle as a dark particle, which is unobservable. As a result, most of the experimental findings do not provide a good reference for ALRM. The value of right-handed coupling constant g_R has a significant impact on the constraints of W' particle mass. When the value of g_R is relatively small, the lower limit of W' mass might be smaller. In the ALRM adopted in this paper, the allowed range of g_R for the coupling with right-handed gauge bosons is $0.37 \sim 0.765$, where the lower limit of the allowed range comes from the theoretical restriction that g_R/g_L must be larger than $\tan\theta_W$ [39, 40], and the upper limit comes from the phenomenological specification of g_R [10].

III. W' BOSON PRODUCTION AND DECAY AT FUTURE MUON COLLIDER

In this chapter, we will investigate the properties of the W' with the pair production through different processes at the future μ collider. The μ collider is a proposed lepton collider with great potential for the future, and the related contents can be found in references [41−44]. We have chosen the process $\mu^+\mu^- \to W'^+W'^- \to e^+e^- n_e \bar{n}_e$ as our main subject in this study. Before delving into the specific process, we firstly explore all the decay branching ratios of the W' particle within this model, which will help us identify the main decay channels of the W' and analyze them to explore the various properties of it.

A. The decay of W' boson

In ALRM, similar to the Standard Model, gauge bosons can decay into leptons or quarks. Due to the pres-
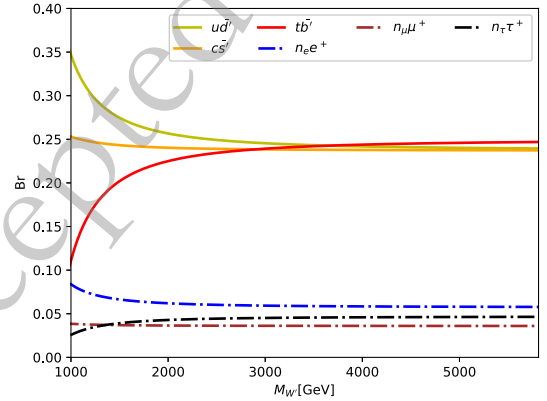
Fig. 1. (color online) Decay branching ratios of W'.

ence of a larger number of new particles in this model, the decay channels of the W' boson are more complicated than the gauge particles in the Standard Model. The main decay channels of W' particle are included in figure 1. Due to the W' particle's large mass, it can decay into a wider array of final states. The masses of the new particles involved are set as $M_{d',n_e} = 300$ GeV, $M_{s',n_\mu} = 500$ GeV, $M_{t',n_\tau} = 700$ GeV.

The coupling strength of W' particle decaying into all generations of leptons (e, μ, τ) are set the same for simplicity in this study. When the W' particle mass is less than 2 TeV, the decay branching ratio of the first generation light quarks is the largest. As the increasing of W' particle mass, the decay branching ratio of the third generation are raising. As the mass of W' larger than 3 TeV, the decay branching ratios of quark channels tend to the similar values around 0.25. At the same times the decay branching ratios of electron channel is about 0.06, and the muon channel and tau channel are slightly smaller than 0.05.

Actually, the decay process of W' also involves flavor-changing processes, but their decay branching ratios are less than 0.01 in our studied parameter spaces. Thus they are not plotted in figure 1. The interesting studies on the flavor-changing processes can be found in [45−47], which is out of our reach in this work.
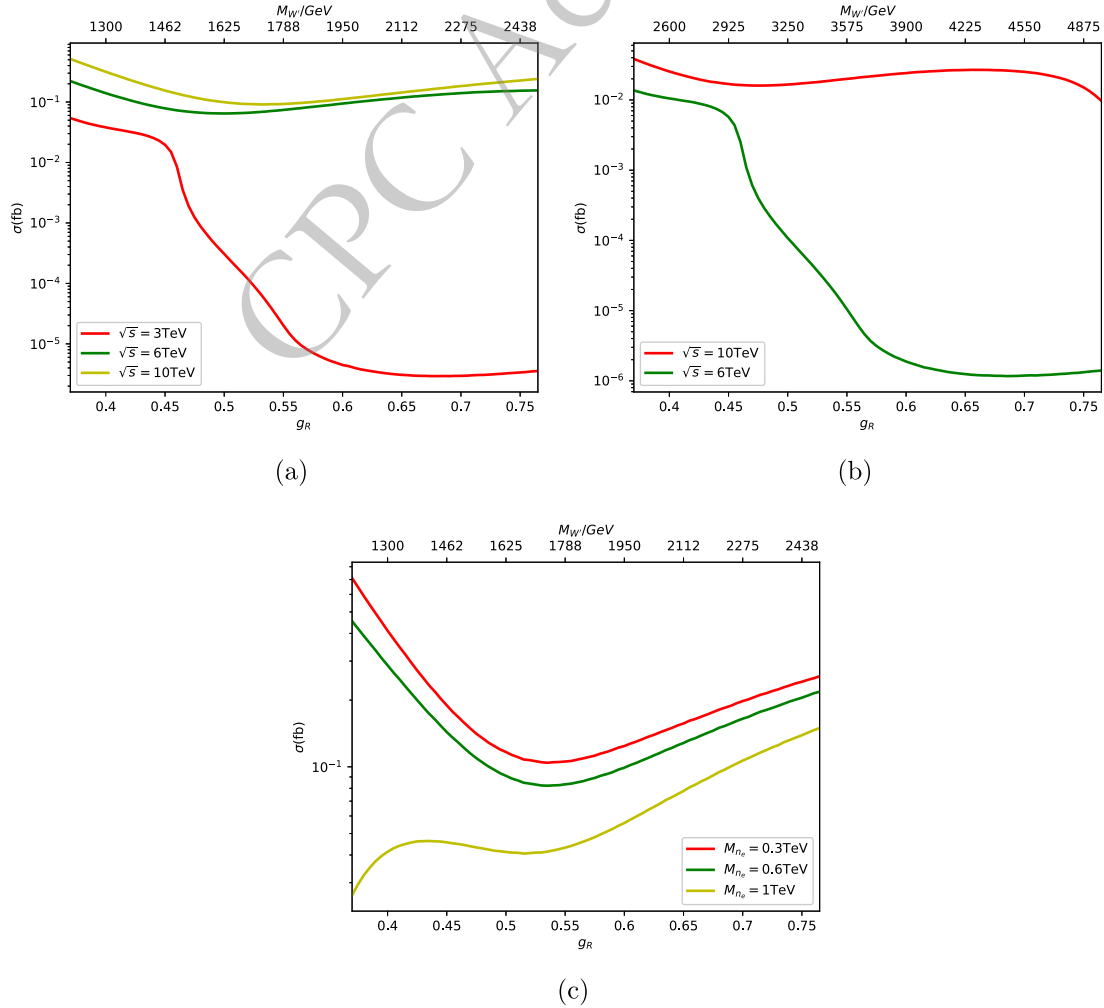
B. The process of $\mu^+\mu^- \to W'^+W'^- \to e^-e^+ n_e \bar{n}_e$

We focus on the process of W' decay into a pair of

light leptons, i.e., $\mu^+\mu^- \to W'^+W'^- \to e^+e^-n_e\bar{n}_e$. Although the branching ratios for quark final states are significantly larger than those for lepton final states in the previous studies, we have chosen the latter as the target process in this part for the following reasons. Firstly, the final charged leptons as free particles can more easily be measured than the quarks at colliders. Secondly, the right-handed neutrinos produced can be considered as candidates for dark matter, and it leads the large missing transverse momentum as a signature. Last but not least, in our chosen decay chains it includes the couplings of W' and leptons without the quarks, which is benefit for the study of W' and leptons interactions. All of our results are obtained through Monte Carlo simulations [48, 49].

1. *Cross Section*

Figure 2 shows the cross section distribution of $\mu^+\mu^- \to W'^+W'^- \to e^+e^-n_e\bar{n}_e$ process with the right-handed coupling constant g_R. The plot in figure 2 (a) shows the

cross section with different collision energies of 3, 6, and 10 TeV (represented by red, green, and yellow solid lines, respectively). In the ALRM model, the mass of the W' boson is determined by the coupling constant g_R and the vacuum expectation value according to equation (5), so when the vacuum expectation value is fixed, there is a one-to-one correspondence between the right-handed coupling constant g_R and the mass of the W' particle. Therefore, we have added coordinate axes for both g_R and $M_{W'}$ parameters in the figure. The vacuum expectation value is fixed at 6.5 TeV in this figure. When the collision energy is 3 TeV, the cross section rapidly decreases with $g_R = 0.45$, where the mass of the W' boson is close to 1.5 TeV. Since it is approaching the threshold for W' pair production. When g_R reaches its maximum of 0.765, the corresponding mass of the W' boson produced is about 2.4 TeV, which means the W' bosons can be on shell produced with collision energy of 6 or 10 TeV in the whole studied parameter spaces. The cross section at collision energy of 6 TeV or 10 TeV exhibits a trend of first

(a)

(b)

(c)
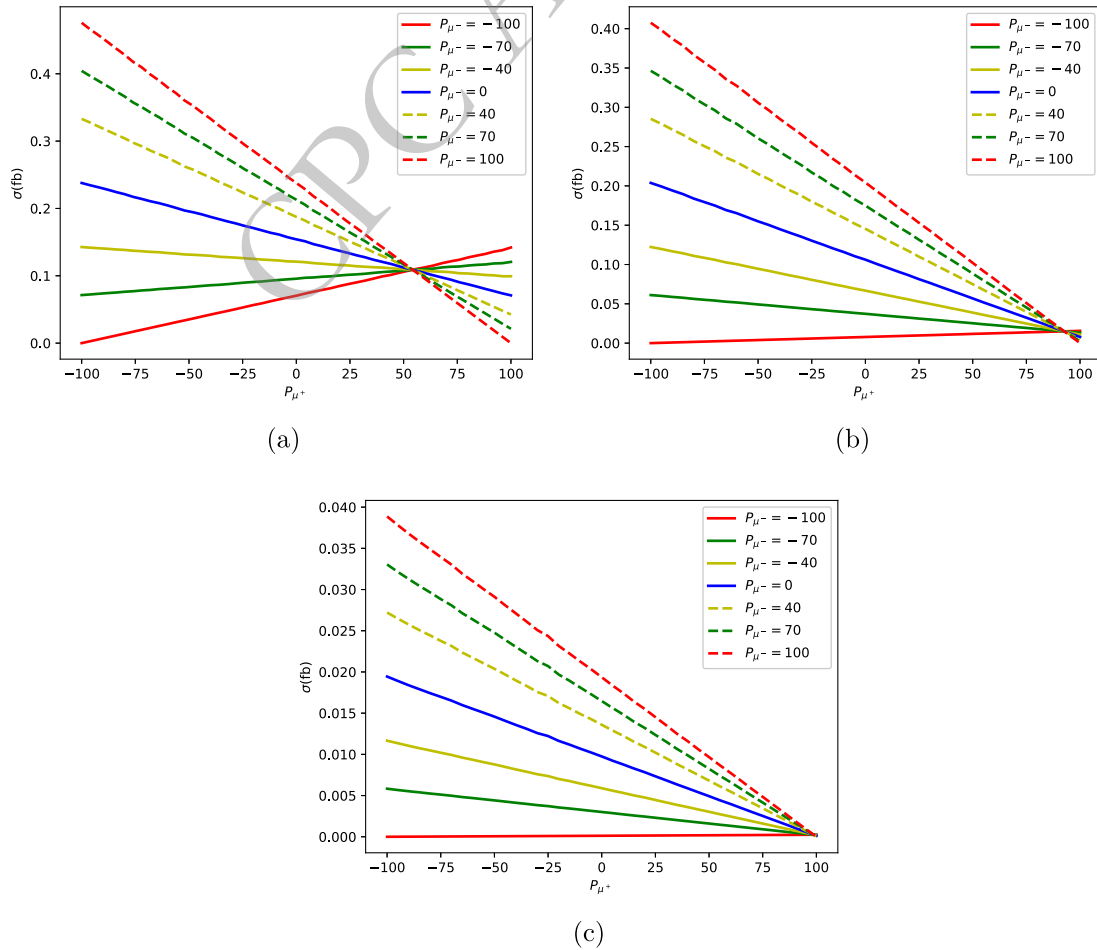
Fig. 2.   (color online) cross section for the process $\mu^+\mu^- \to W'^+W'^- \to e^+e^-n_e\bar{n}_e$ versus different couplings in figure (a) and (b). And figure (c) shows the cross section of the same process versus different M_{n_e} with $\sqrt{s} = 10$ TeV.

rising and then falling with the increasing of g_R. This phenomena are due to the dual impact of g_R and the mass of W'.

The plot in figure 2 (b) also shows the cross section for $\mu^+\mu^- \to W'^+W'^- \to e^+e^-n_e\bar{n}_e$ process at different collision energies of 6 and 10 TeV with different g_R. The difference between (b) and (a) lies in the fact that we have chosen different vacuum expectation values of the Higgs field, which leads to different W' particle masses with same coupling constant g_r. The vacuum expectation value is fixed at 13 TeV in figure 2 (b). Figure 2 (c) shows the cross section of $\mu^+\mu^- \to W'^+W'^- \to e^+e^-n_e\bar{n}_e$ process at a collision energy of 10 TeV with different neutrino mass scenarios (the red, green, and yellow solid lines represent the cross sections when the neutrino masses are 0.3, 0.6 and 1 TeV, respectively). In this plot, the vacuum expectation value also remains 6.5 TeV. When the neutrino mass is 0.3 (1) TeV, the cross section is about 0.41 (0.041) fb with $g_R = 0.4$ and 0.24 (0.14) fb with $g_R = 0.75$. The neutrino mass has a significant impact on the cross section in the process of leptonic decaying channels.

The polarization of the initial state particles can have a significant impact on the production of W' pairs. Figure 3 (a) illustrates the cross section varies with different polarization of the initial muons through $\mu^+\mu^- \to W'^+W'^- \to e^+e^-n_e\bar{n}_e$ process under the condition of collision energy of 10 TeV and $m_{W'} = 2$ TeV. The polarization varies from fully left-handed ($P_\mu = -100$) to fully right-handed ($P_\mu = 100$) with some typical values in the plots. Each curve in the figure 3 represents a fixed polarization state of the μ^- particle, with the polarization degree of the μ^+ particle varying along the x-axis. The lines in figure 3 (a) reveals an important physics phenomenon. When the polarization of μ^- is fixed, the cross section varies with the polarization of μ^+ in different ways. When the polarization of μ^- is 100, the cross section continuously decreases with the positive increase of μ^+ polarization. When the polarization of μ^- is -100, the trend of the cross section continuously increases. Therefore, it provides the maximum and minimum values of the cross section in this process for the polarization conditions $(P_{\mu^+}, P_{\mu^-}) = (-100, 100)$ and $(P_{\mu^+}, P_{\mu^-}) = (-100, -100)$. In particular, when the μ^- particles are fully polarized

Fig. 3. (color online) Cross section distributions of $\mu^+\mu^- \to W'^+W'^- \to e^+e^-n_e\bar{n}_e$ process with various initial state polarization for $M_{W'} = 2$ TeV (a), $M_{W'} = 3.5$ TeV (b), and $M_{W'} = 5$ TeV (c) at 10 TeV muon collider.

($P_{\mu^-} = \pm 100$), the trends in the plot become more pronounced, providing us with important clues about the characteristics of particle interactions under extreme polarization conditions. This is crucial for subsequent work in enhancing signal production.

Figure 3 (b) and (c) is the same distribution as (a) but $M_{W'} = 3.5$ and 5 TeV. When the mass of W' increases, the cross section changes significantly for $P_{\mu^-} < 0$. When P_{μ^-} equals to -40, the cross section for $M_{W'}$ at 2 TeV increases gradually with the positive polarization of μ^+, but for $M_{W'}$ at 3.5 TeV, the cross section shows a decreasing trend. It is important to note that when $M_{W'}$ is 3.5 and 5 TeV with $P_{\mu^-} = -100$, the cross section continuously increases with the positive polarization of μ^+, but the increase is relatively small.

2. *Angular Distribution*

The angular distribution of the final particle is an important observable for the study of the properties of W' boson. The formula for the angular distribution is as follows,

$$\cos\theta = \frac{\boldsymbol{p}_f^* \cdot \boldsymbol{p}_i}{|\boldsymbol{p}_f^*| \cdot |\boldsymbol{p}_i|}, \tag{8}$$

where $\boldsymbol{p}_f^*$ and $\boldsymbol{p}_i$ are the three momentum of the final and initial particle, respectively.

In our work, the influence of angular distribution variables is mainly focused on two aspects: the spin polarization of the incident particles and the variation of coupling constants [50], which are essentially the result of the combined action of angular momentum conservation and chirality rules. First, changes in the spin polarization state of incident particles affect the polarization direction of intermediate-state particles. This leads to a preference for a specific direction in the decay process of intermediate particles into final-state particles. Therefore, different polarization states will influence the angular distribution of the final-state particles. Second, the change in angular distribution is caused by the chiral asymmetry of the coupling strength which is related to the right-handed coupling g_R and different vacuum expectation value in the model. The V-A structure of the gauge interaction in the model leads to coupling differences between left-handed and right-handed particles, resulting in an asymmetric production process of final-state particles.

Figure 4 (a) shows the effects of different coupling constant g_R on the angular distributions between μ^- and e^- particles of process $\mu^+\mu^- \to W'^+ W'^- \to e^+ e^- n_e \bar{n}_e$, with an vacuum expectation value of 6.5 TeV. For the unpolarized initial state, the coupling constant g_R has a significant impact on the angular distribution of the final state particles. When the value of the right-handed coupling constant g_R is 0.37, the angular distribution is symmetric

in the plot. And as the coupling constant increases, one can clearly observe an increase in the asymmetry of the angular distribution of the final state particles. When the right-handed coupling constant is 0.765, the cross section has a clear enhancement with $\cos\theta$ closing to one.

Figure 4 (b) shows the impact of polarization of the initial μ^- on the final electron angular distributions. As the polarization strength increases, the changes of the angular distributions become more pronounced. Figure 4 (c) shows the angular distributions resulting from polarized both initial μ^- and μ^+. We can see that compared to Figure 4 (b), polarizing both particles to the same extent on the basis of figure 4 (b) does not have a significant impact on the angular distribution.
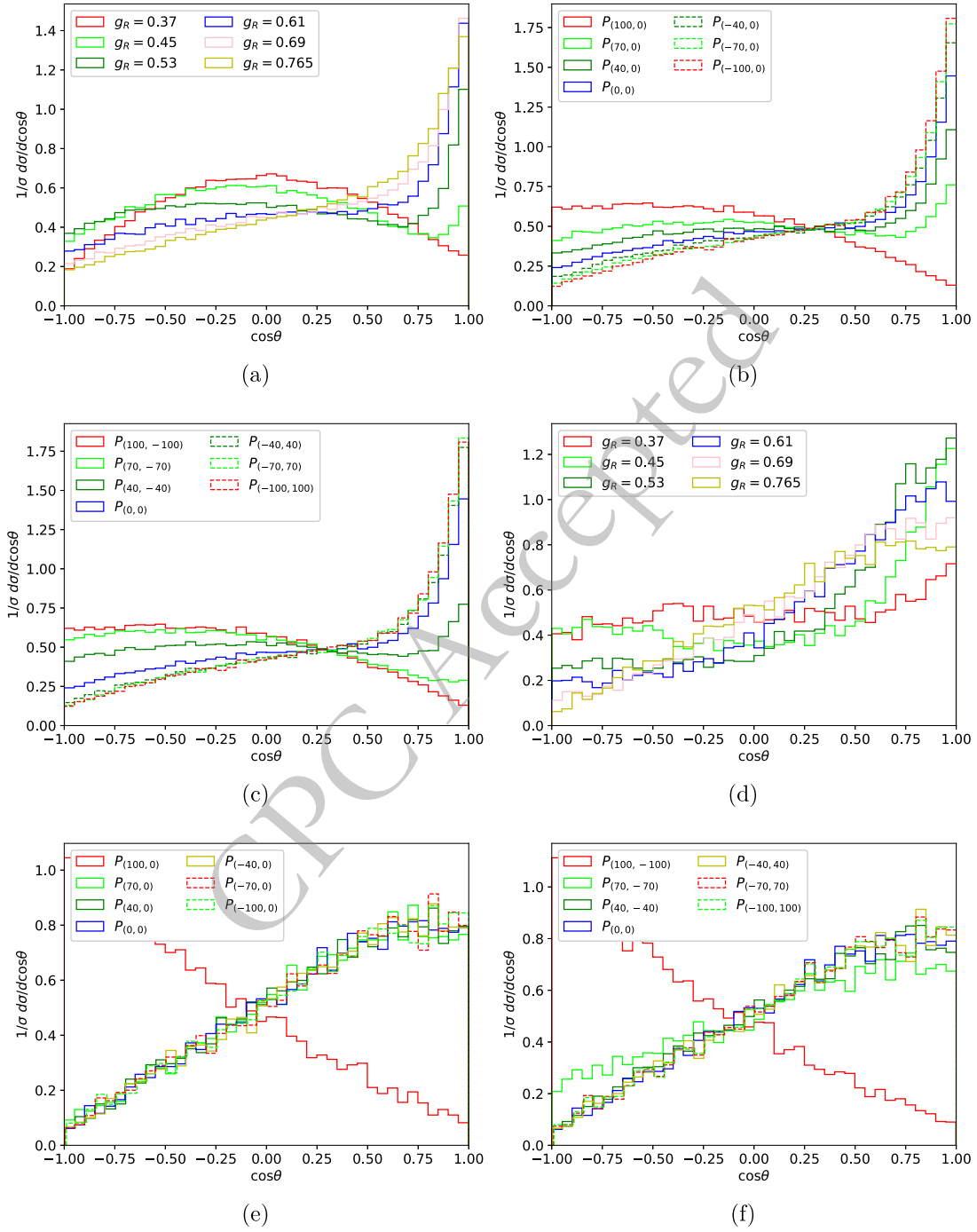
Figure 4 (d) also shows the angular distributions of final state electrons with unpolarized initial particles for the vacuum expectation value of 13 TeV. Figure 4 (e) and (f) shows the angular distribution of the final state particles in the polarized condition when the W' mass is 5 TeV. The results show that the angular distributions tend to the same shapes with various initial polarization except for the case of P_{μ^+} extremely close to 100.

The mass of W' has significant effects on the angular distribution of final electrons from $\mu^+\mu^- \to W'^+ W'^- \to e^+ e^- n_e \bar{n}_e$ process as shown in Figure 5. The mass of W' has been set at 2 TeV, 3.5 TeV and 5 TeV with the collision energy of 10 TeV. As the increase of W' mass, the asymmetry of the angular distribution becomes more obvious. Moreover, the angular distributions tend to consistency with the mass of W' increasing to the threshold of the W' pair production and the effects of different g_R values have been suppressed with the W' mass increasing.

Forward-backward asymmetry is a specific aspect of angular distribution that describes the difference in the emission probabilities of particles in the forward $(\cos\theta \geq 0)$ and backward $(\cos\theta < 0)$ hemispheres. We define the formula for A_{FB} as follows,

$$A_{FB} = \frac{\sigma(\cos\theta \geq 0) - \sigma(\cos\theta < 0)}{\sigma(\cos\theta \geq 0) + \sigma(\cos\theta < 0)}. \tag{9}$$

One of the key studies of the work in the angular distribution section lies in establishing a relationship between A_{FB} and the coupling constants of the W' particle. When a large number of background processes are present in the process, they can interfere with the variation characteristics of the signal process. Additionally, regarding the background information mentioned above: in the significance calculation process, the three background processes we mentioned are $\mu^+\mu^- \to W^+ W^- \to e^+ e^- \nu_e \bar{\nu}_e, \mu^+\mu^- \to ZZ \to e^+ e^- \nu_e \bar{\nu}_e, \mu^+\mu^- \to Z\nu_m \bar{\nu}_m, (Z \to e^+ e^-)$. When the cut conditions in the paper are satisfied, the signal process can be completely separated from the background processes, and at this point, the background has little effect on the angular distribution. Therefore,
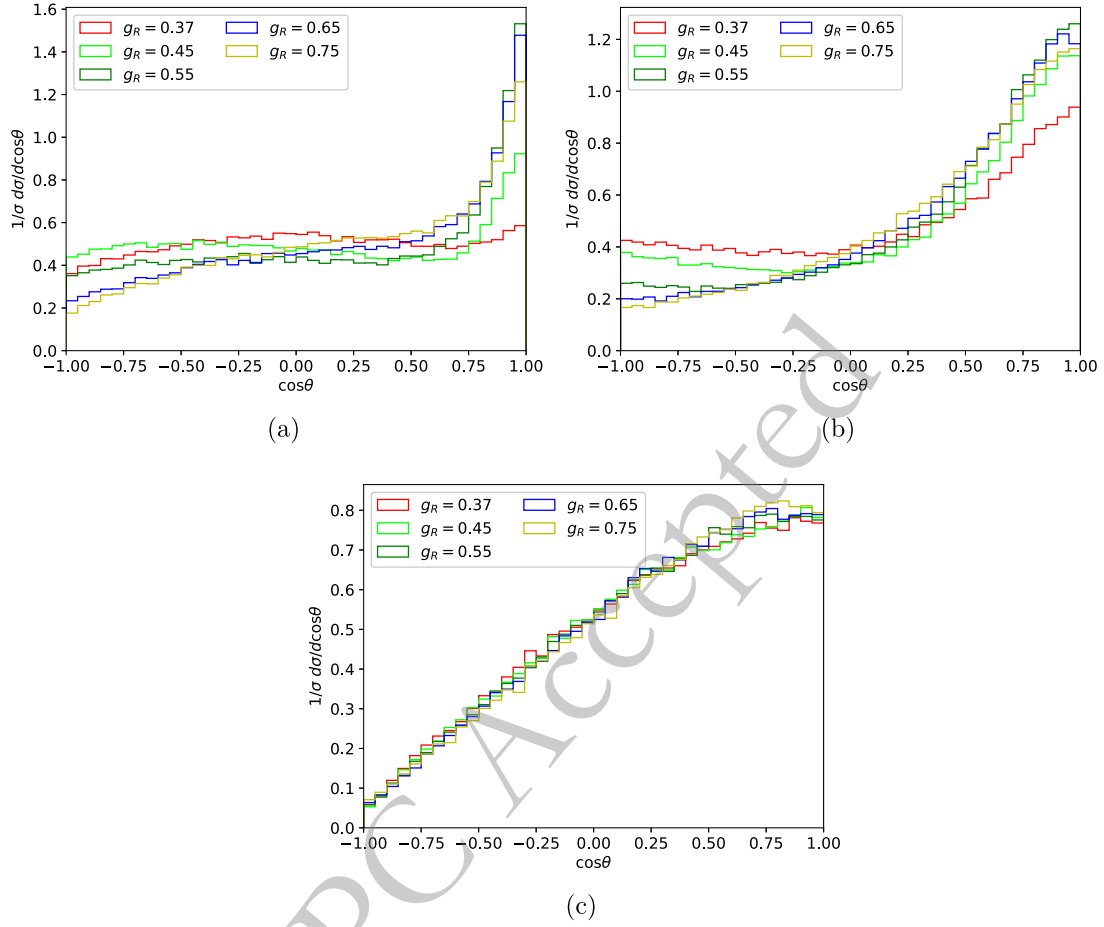
Fig. 4. (color online) The angular distributions between μ^- and e^- of the unpolarized and polarized processes $\mu^+\mu^- \to W'^+W'^- \to e^+e^-n_e\bar{n}_e$ corresponding to the collision energy of 10 TeV. The vacuum expectation is 6.5 TeV in figure (a), and 13 TeV in figure (d). The fixed mass of W' is 2 TeV in figure (b) and (c) with $g_R = 0.65$, and $M_{W'} = 5$TeV, $g_R = 0.765$ for (e) (f).

based on the complete separation of the signal process, we only simulated the angular distribution of the final-state particles of the signal process.

Table 3 presents the forward-backward asymmetry of final electrons in the process of $\mu^+\mu^- \to W'^+W'^- \to e^+e^-n_e\bar{n}_e$ with various right-handed couplings and polarization of initial states. The asymmetry is 0.005 (0.37) with

$g_R = 0.37$ (0.765) for a fixed vacuum expectation value of 6.5 TeV. And the asymmetry varies from -0.24 to 0.42 with the polarization of $P_{\mu^+} = 100$ to $P_{\mu^+} = -100$. Comparing the results of the second and third columns, one can find that the inversed polarization of μ^- has slightly influence on the asymmetries.

Fig. 5. The angular distributions between μ^- and e^- of the unpolarized processes $\mu^+\mu^- \to W'^+W'^- \to e^+e^-n_e\bar{n}_e$ corresponding to the collision energy of 10 TeV with $M_{W'} = 2$ TeV (a), 3.5 TeV (b) and 5 TeV (c), respectively.

Table 3. The forward-backward asymmetry with different conditions for $\mu^+\mu^- \to W'^+W'^- \to e^+e^-n_e\bar{n}_e$. The vacuum expectation value is fixed at 6.5 TeV in the first column, and $M_{W'}$ is 2 TeV in the second and third column.

g_R	A_{FB}	$P_{(P_{\mu^+}, P_{\mu^-})}$	A_{FB}	$P_{(P_{\mu^+}, P_{\mu^-})}$	A_{FB}
0.37	0.005	$(100, 0)$	-0.24	$(100, -100)$	-0.24
0.45	-0.043	$(70, 0)$	0.0016	$(70, -70)$	-0.18
0.53	0.034	$(40, 0)$	0.14	$(40, -40)$	0.013
0.61	0.21	$(-40, 0)$	0.34	$(-40, 40)$	0.39
0.69	0.31	$(-70, 0)$	0.39	$(-70, 70)$	0.41
0.765	0.37	$(-100, 0)$	0.42	$(-100, 100)$	0.42

3. *Significance*

We utilize Monte Carlo simulations [48, 51−53] to simulate collisions for signal and background processes, focusing our study on the di-lepton processes. In our simulations, we pay attention to the signal process with the W' pair production as an intermediate state,

$$\mu^+\mu^- \to W'^+W'^- \to e^+e^-n_e\bar{n}_e. \tag{10}$$

The main background processes include the production of ZZ, WW particles and the VBF process directly constituted by Z and neutrinos. The background processes are shown as follows

$$\mu^+\mu^- \to W^+W^- \to e^+e^-\nu_e\bar{\nu}_e, \tag{11}$$

$$\mu^+\mu^- \to ZZ \to e^+e^-\nu_e\bar{\nu}_e, \tag{12}$$

$$\mu^+\mu^- \to Z\nu_m\bar{\nu}_m, (Z \to e^+e^-). \qquad (13)$$

Where the left-handed or right-handed neutrinos can not be directly detected in the colliders. We treat them as the missing transverse energy.

The signal-to-noise ratio is a measure of the strength of a signal relative to the level of background noise. Another way to compare the signal and backgrounds is the significance. These two values can be expressed from

$$S/B = \frac{\sigma_S}{\sigma_B}, \quad S/\sqrt{B} = \frac{\sigma_S \times I}{\sqrt{\sigma_B \times I}}, \qquad (14)$$

where σ_S represents the cross section of the signal and σ_B represents the cross section of the backgrounds. I represents the integrated luminosity of the collider, which is set as $10ab^{-1}$ in this work.

To distinguish the signal from the backgrounds, we firstly give some kinematic distributions in figure 6. The collision energy is 10 TeV and $m_{W'} = 2$ TeV. Here, P_T represents the transverse momentum of the final state

electrons in figure 6 (a). η is the pseudo-rapidity of electrons in figure 6 (b). Another important parameter is α in figure 6 (c), which is the azimuthal angle of the final state electrons calculated with the angle between the two charged leptons in the transverse plane. The α is defined as:

$$\cos\alpha = \frac{\boldsymbol{p}_{e^+}^* \cdot \boldsymbol{p}_{e^-}}{|\boldsymbol{p}_{e^+}^*| \cdot |\boldsymbol{p}_{e^-}|}, \qquad (15)$$

where p_e denote the three-momentum vectors of the electrons in the relevant frame. The different distribution in Figure 6 (c) between the signal process and background processes is determined by the kinematic characteristics of the collision process. The two background processes with distinct differences are those with intermediate states of Z bosons and W boson pairs, whose Feynman diagrams correspond to the t-channel and s/t-channels [54], respectively. For the large collision energy, the W/Z will be highly boosted, which will cause the distribution has a sharp peak. While for the large mass of the intermediate
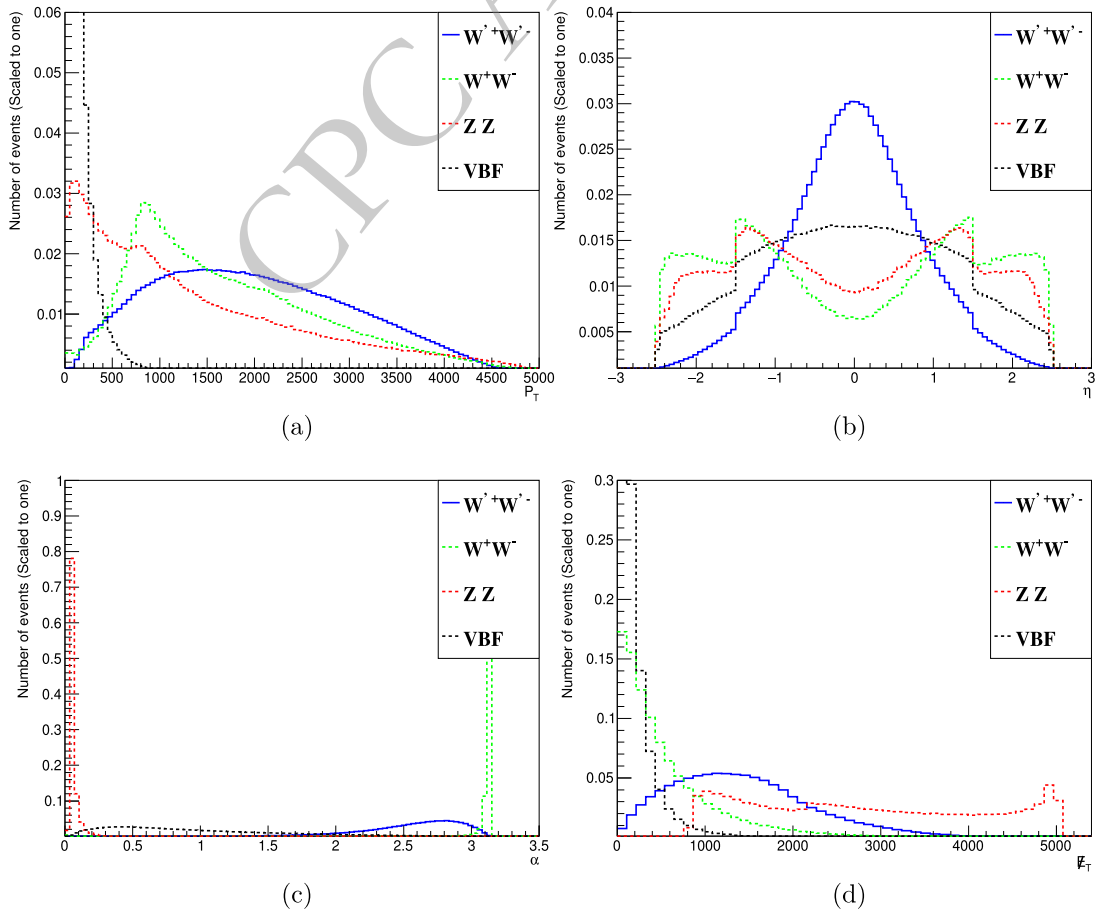
Fig. 6. (color online) The kinematic distributions of the final particles for the signal and background processes before the cuts. (a), (b), (c) represent the transverse momentum P_T, pseudo-rapidity η, correlated angle α between the two charged particles in the final state and (d) is the missing transverse energy $\not{E}_T$.

Table 4. The signal-to-noise ratio and significance after cuts with the mass of W' is 2, 4.5 and 4.8 TeV and the collision energy is 10 TeV, and the integrated luminosity of the collider is set as $10ab^{-1}$. The unit of σ is fb.

$m_{W'}$	cut range	σ_{WW}	σ_{ZZ}	σ_{VBF}	σ_S	$S/\sqrt{B}$	S/B
2TeV	Basic Cut	0.062	0.0016	44.93	0.066	0.0015	0.98
	$P_T > 400\text{GeV}$	0.058	0.00087	0.31	0.061	0.16	10.02
	$0.5 < \alpha < 3.1$	0.0036	0	0	0.061	17	101.62
4.5TeV	Basic Cut	0.062	0.0016	44.93	0.0095	2.1×10^{-4}	0.14
	$600 < P_T < 3700\text{GeV}$	0.047	0.00056	0.089	0.0091	0.066	2.45
	$0.5 < \alpha < 3$	0.00093	0	0	0.0088	9.47	28.91
4.8TeV	Basic Cut	0.062	0.0016	44.93	0.0053	1.2×10^{-4}	0.079
	$600 < P_T < 3500\text{GeV}$	0.046	0.00054	0.089	0.0051	0.038	1.38
	$0.5 < \alpha < 3$	0.00091	0	0	0.0049	5.42	16.35

particle of W' in the signal process as well as the heavy neutrino mass, the boost effects will be small, thus the distributions will be much flatter in the signal process. And the last one in figure 6 (d) is $\not{E}_T$, which represent the transverse energy carried away by the neutrinos. From these distributions we can find the discrepancy of the signal and background processes.

We attempted to the search of W' pair production with different masses of 2 TeV, 4.5 TeV and 4.8 TeV at a collision energy of 10 TeV. Different cuts are applied to enhance the significance. The results are listed in Table 4 in details. The basic cuts are defined as that the number of final-state electrons must be two, and both of them are charge conjugates with the transverse momentum $P_T > 10$ GeV. When the cuts on the final-state electrons are set as $P_T > 400$ GeV and $0.5 < \alpha < 3.1$, the signal-to-noise ratio can reach 17 and the significance can reach 101.62 for 2 TeV W'. When the W' mass is up to 4.5 TeV, the cuts are changed to $600 < P_T < 3700$ GeV and $0.5 < \alpha < 3$. The signal-to-noise ratio is 9.47 and the significance value is 28.91. The results of $m_{W'} = 4.8$ TeV is given with the cuts of $600 < P_T < 3500$ GeV and $0.5 < \alpha < 3$. The signal-to-noise ratio is 5.42 and the significance value is 16.35. With the mass of W' close to 5 TeV as the threshold of pair production for collision energy of 10 TeV, the cross section will decrease sharply with increasing mass, thus the significance will decrease obviously.

IV. SUMMARY

Extra charged gauge bosons beyond the Standard Model have always been a topic of interest. Future muon colliders, due to their high center-of-mass energies, have a significant advantage in discovering heavy particles. In this paper, we choose the ALRM model to study the $\mu^+\mu^- \to W'^+W'^- \to e^+e^-n_e\bar{n}_e$ process and explore the prop-

erties of W'. In this process, we examine the cross section distribution, angular distribution, and forward-backward asymmetry for polarized and unpolarized scenarios of W' particles at different masses.

We have conducted an in-depth study of the cross section distribution of the process $\mu^+\mu^- \to W'^+W'^- \to e^+e^-n_e\bar{n}_e$ at different collision energies. The cross section can reach 0.2 fb in a 10 TeV collider, which is correlated to the combined effects of g_R and the W' mass. We also investigate the angle distributions of the initial-state muon and final-state electron for different W' masses. With a fixed W' mass, the asymmetry of the angular distribution gradually strengthens as the g_R increasing. With the same coupling strength, the changes in W' mass also greatly affect the angular distribution, but the overall trend remains consistent. We also investigate the cross section distribution and angular distribution for the polarized initial state conditions. When the μ^- polarization is different, the distributions of cross section also show significant changes with the W' mass lower than half of the collision energy. But the polarization has slight effects on the angular distributions when the W' mass close to the threshold of pair production except for the case of P_{μ^+} extremely close to 100. The forward-backward asymmetry defined from the angular distribution is an effective observable to study the interaction of W' coupling to leptons. We also give the search of W' pair production at the muon collider with the mainly backgrounds of ZZ, WW and VBF processes. After applying the suitable kinematic cuts, the significance can beyond 5σ for W' boson with mass of 4.8 TeV at the 10 TeV muon colliders. The study of extra gauge particles is an important part of the new physics beyond standard model. Searches on the pair production of W' at the future muon collider provide new perspective for the new physics models.

References

[1] A. A. Andrianov, N. V. Borisov, M. V. Ioffe, and M. I. Eides, Theor. Math. Phys. **61**, 965 (1984)

[2] M. V. Ioffe and A. I. Neelov, J. Phys. A **33**, 1581 (2000), arXiv: quant-ph/0001063

[3] N. Seiberg, Nucl. Phys. B **435**, 129 (1995), arXiv: hep-th/9411149

[4] C. H. Clemens and S. Raby, JHEP **04**, 004, arXiv:2001.10047[hep-th].

[5] J. C. Baez and J. Huerta, Bull. Am. Math. Soc. **47**, 483 (2010), arXiv: 0904.1556[hep-th]

[6] D. Croon, T. E. Gonzalo, L. Graf, N. Košnik, and G. White, Front. in Phys. **7**, 76 (2019), arXiv: 1903.04977[hep-ph]

[7] G. Senjanovic and R. N. Mohapatra, Phys. Rev. D **12**, 1502 (1975)

[8] J. Liu, Z.-L. Han, Y. Jin, and H. Li, JHEP **12**, 057, arXiv:2207.07382[hep-ph].

[9] R.-Y. He, J.-Q. Huang, J.-Y. Xu, F.-X. Yang, Z.-L. Han, and F.-L. Shao, Chin. Phys. C **48**, 093102 (2024), arXiv: 2401.14687[hep-ph]

[10] M. Frank, B. Fuks, and O. Özdal, JHEP **04**, 116, arXiv:1911.12883[hep-ph].

[11] M. Ashry and S. Khalil, Phys. Rev. D **91**, 015009 (2015), [Addendum: Phys.Rev.D 96, 059901 (2017)], arXiv:1310.3315[hep-ph].

[12] T. Aaltonen *et al.* (CDF), Science **376**, 170 (2022)

[13] D. Van Loi and P. Van Dong, Eur. Phys. J. C **83**, 56 (2023), arXiv: 2206.10100[hep-ph]

[14] P. S. B. Dev, R. N. Mohapatra, and Y. Zhang, Mod. Phys. Lett. A **32**, 1740007 (2017), arXiv: 1610.05738[hep-ph]

[15] M. Frank, C. Majumdar, P. Poulose, S Senapati, and U. A. Yajnik, JHEP **12**, 032, arXiv:2211.04286[hep-ph].

[16] Z. Lu, H. Li, Z.-L. Han, Z.-G. Si, and L. Zhao, Sci. China Phys. Mech. Astron. **67**, 231012 (2024), arXiv: 2312.17427[hep-ph]

[17] X. Yin, H. Li, Y. Jin, Z. Han, and Z. Lu, Chin. Phys. C **46**, 053106 (2022), arXiv: 2112.13975[hep-ph]

[18] X. Gong, H.-L. Li, C.-F. Qiao, Z.-G. Si, and Z.-J. Yang, Phys. Rev. D **89**, 055022 (2014), arXiv: 1403.0347[hep-ph]

[19] J. Kriewald, M. Nemevšek, and F. Nesti, (2024), arXiv:2403.07756[hep-ph].

[20] M. Frank, B. Fuks, A. Jueid, S. Moretti, and O. Ozdal, JHEP **02**, 150, arXiv:2312.08521 [hep-ph].

[21] N. Vignaroli, JHEP **10**, 121, arXiv:2304.12362[hep-ph].

[22] S. F. Solera, A. Pich, and L. Vale Silva, JHEP **02**, 027, arXiv:2309.06094[hep-ph].

[23] K. Korshynska, M. Löschner, M. Marinichenko, K. Mękała, and J. Reuter, Eur. Phys. J. C **84**, 568 (2024), arXiv: 2402.18460[hep-ph]

[24] Y. Achiman and B. Stech, Phys. Lett. B **77**, 389 (1978)

[25] F. Gursey, P. Ramond, and P. Sikivie, Phys. Lett. B **60**, 177 (1976)

[26] M. Mitra, R. Ruiz, D. J. Scott, and M. Spannowsky, Phys. Rev. D **94**, 095016 (2016), arXiv: 1607.03504[hep-ph]

[27] E. Ma, Phys. Rev. D **85**, 091701 (2012), arXiv: 1202.5828[hep-ph]

[28] M. Frank, C. Majumdar, P. Poulose, S. Senapati, and U. A. Yajnik, (2024), arXiv:2402.04192 [hep-ph].

[29] R. N. Mohapatra and D. P. Sidhu, Phys. Rev. D **16**, 2843 (1977)

[30] M. Aaboud *et al.* (ATLAS), Phys. Lett. B **798**, 134942 (2019), arXiv: 1904.12679[hep-ex]

[31] M. Aaboud *et al.* (ATLAS), Phys. Rev. Lett. **120**, 161802 (2018), arXiv: 1801.06992[hep-ex]

[32] A. M. Sirunyan *et al.* (CMS), JHEP **05**, 033, arXiv:1911.03947[hep-ex].

[33] A. M. Sirunyan *et al.* (CMS), JHEP **06**, 128, arXiv:1803.11133[hep-ex].

[34] A. M. Sirunyan *et al.* (CMS), Phys. Lett. B **792**, 107 (2019), arXiv: 1807.11421[hep-ex]

[35] A. Tumasyan *et al.* (CMS), JHEP **07**, 067, arXiv:2202.06075[hep-ex].

[36] A. Tumasyan *et al.* (CMS), JHEP **04**, 047, arXiv:2112.03949[hep-ex].

[37] G. Aad *et al.* (ATLAS), Phys. Rev. D **109**, 112008 (2024), arXiv: 2402.16576[hep-ex]

[38] M. Aaboud *et al.* (ATLAS), Phys. Lett. B **798**, 134942 (2019), arXiv: 1904.12679[hep-ex]

[39] J. Brehmer, J. Hewett, J. Kopp, T. Rizzo, and J. Tattersall, JHEP **10**, 182, arXiv:1507.00013 [hep-ph].

[40] P. S. B. Dev, R. N. Mohapatra, and Y. Zhang, JHEP **05**, 174, arXiv:1602.05947[hep-ph].

[41] C. Accettura *et al.*, Eur. Phys. J. C **83**, 864 (2023), [Erratum: Eur.Phys.J.C 84, 36 (2024)], arXiv:2303.08533[physics.acc-ph].

[42] M. Casarsa, D. Lucchesi, and L. Sestini 10.1146/annurev-nucl-102622-011319 (2023), arXiv:2311.03280[hep-ex].

[43] C. Accettura *et al.* (International Muon Collider), (2024), arXiv:2407.12450[physics.acc-ph].

[44] A. Abada *et al.* (FCC), Eur. Phys. J. ST **228**, 261 (2019)

[45] S. P. Das, F. F. Deppisch, O. Kittel, and J. W. F. Valle, Phys. Rev. D **86**, 055006 (2012), arXiv: 1206.0256[hep-ph]

[46] M.-C. Chen and H.-B. Yu, Phys. Lett. B **672**, 253 (2009), arXiv: 0804.2503[hep-ph]

[47] T. Han, I. Lewis, R. Ruiz, and Z.-g. Si, Phys. Rev. D **87**, 035011 (2013), [Erratum: Phys.Rev.D 87, 039906 (2013)], arXiv:1211.6447[hep-ph].

[48] J. Alwall, R. Frederix, S. Frixione, V. Hirschi, F. Maltoni, O. Mattelaer, H. S. Shao, T. Stelzer, P. Torrielli, and M. Zaro, JHEP **07**, 079, arXiv:1405.0301[hep-ph].

[49] O. Mattelaer and K. Ostrolenk, Eur. Phys. J. C **81**, 435 (2021), arXiv: 2102.00773[hep-ph]

[50] S. Navas *et al.* (Particle Data Group), Phys. Rev. D **110**, 030001 (2024)

[51] J.-C. Walter and G. Barkema, Physica A: Statistical Mechanics and its Applications **418**, 78 (2015)

[52] M. P. Allen, Introduction to monte carlo simulation, in *Observation, Prediction and Simulation of Phase Transitions in Complex Fluids*, edited by M. Baus, L. F. Rull, and J.-P. Ryckaert (Springer Netherlands, Dordrecht, 1995) pp. 339–356.

[53] S. Frixione, O. Mattelaer, M. Zaro, and X. Zhao, (2021), arXiv:2108.10261[hep-ph].

[54] D. Griffiths, Introduction to elementary particles (2008).